Free boundary ballooning mode representation

L. J. Zheng
Institute for Fusion Studies, University of Texas at Austin, Austin, Texas 78712, USA

(Received 22 May 2012; accepted 1 October 2012; published online 15 October 2012)

A new type of ballooning mode invariance is found in this paper. Application of this invariance is shown to be able to reduce the two-dimensional problem of free boundary high n modes, such as the peeling-ballooning modes, to a one-dimensional problem. Here, n is toroidal mode number. In contrast to the conventional ballooning representation, which requires the translational invariance of the Fourier components of the perturbations, the new invariance reflects that the independent solutions of the high n mode equations are translationally invariant from one radial interval surrounding a single singular surface to the other intervals. The conventional ballooning mode invariance breaks down at the vicinity of plasma edge, since the Fourier components with rational surfaces in vacuum region are completely different from those with rational surfaces in plasma region. But, the new type of invariance remains valid. This overcomes the limitation of the conventional ballooning mode representation for studying free boundary modes. © *2012 American Institute of Physics*. [http://dx.doi.org/10.1063/1.4759012]

I. INTRODUCTION

The conventional ballooning mode representation has been proved to be a successful theory in reducing the two-dimensional (2D) problem of high n ballooning modes into a one-dimensional (1D) problem for internal mode cases.[1–3] Here, n is toroidal mode number. Subsequently, the uniqueness and inversion of the ballooning representation are proved in Ref. 4.

It is desirable if the ballooning mode representation for internal modes can be extended for external modes. Efforts in this direction have been made, since the peeling-ballooning modes were brought to attention in Refs. 5 and 6. However, those efforts retain the conventional ballooning mode invariance assumption in the lowest order, while the free boundary feature is only taken into account in the next order for determining the envelope of Fourier components. In fact, the conventional ballooning representation requires the translational invariance of Fourier's components. This invariance breaks down in the lowest order in edge plasma region. This can be seen from the difference between the interchange and peeling modes.[7–9] The behavior of Fourier components with singular layers being in the plasma region is completely different from that with singular layers being in the vacuum region. Note that the infinities are regarded as singular layers as well in our discussion. If the singular layer is present in the plasma region, only the small solution is allowed at the layer.[7] In the contrary, if the singular layer is present in the vacuum region, the large solution can be accepted. Note that peeling modes are characterized by the presence of singular layer in the vacuum region, so that the large solution emerges at the singular layer.[8,9] It is because of this feature that the stability condition for peeling modes becomes more stringent than that for interchange modes. Therefore, to keep the key peeling effect, one cannot apply the conventional ballooning invariance for external modes.

In this paper, we show that there is a more fundamental type of invariance. This type of invariance relies solo on the scale difference between the distance of mode rational surfaces and equilibrium scale length and is independent of sharp boundary changes, like plasma-vacuum interface. Note that the solution of the set of linear differential equations can be generally expressed as the linear combination of independent solutions. This decomposition method has been widely used in plasma stability analyses.[10] As soon as the scale separation between equilibrium and perturbation remains valid, the independent solutions of the high n mode equations are translationally invariant from one radial interval surrounding a single singular surface to other intervals. Therefore, with the independent solutions being calculated in one radial interval, the independent solutions in the rest intervals can be readily obtained by applying the translational invariance. The independent solutions in all intervals can be subsequently used to make continuous connections between the intervals and to fit any types of boundary conditions, including that for plasma-vacuum interface. Note that the computation effort for all Fourier components in one radial interval is equivalent to that for a single Fourier component in the whole radial coordinate domain. Therefore, by applying the variance of independent solutions, one can reduce the 2D free boundary ballooning mode problem into a 1D one.

The paper is arranged as follows: In Sec. II, the basic set of equations is described. In Sec. III, an alternative description of the conventional ballooning mode representation for internal modes is given. In Sec. IV, the 1D theory for free boundary ballooning modes is described. In Sec. V, the first order theory is presented. The conclusions and discussion are given in the last section. The Appendix is also introduced to explain the free boundary ballooning formalism in a reduced model.

II. THE BASIC SET OF EQUATIONS

To be specific, we use the so-called s-α equilibrium model to describe the ballooning representation,[1] where $s = d\ln q/d\ln r$ denotes magnetic shear and $\alpha = -(2Rq^2/B^2)(dP/dr)$ represents the normalized plasma pressure. Here, q is the safety

factor, R and r represents respectively major and minor radii, P is plasma pressure, and B denotes magnetic field. In this equilibrium model, the plasma energy can be written as[5]

$$\begin{aligned}\delta W_f = -\frac{2\pi^2 B}{nq'R^3B_p^2q}\sum_m \int_\Delta^{+\infty} dx\ u_m^*\Big\{ & s^2[(x-M)^2+\gamma^2]\frac{d^2u_m}{dx^2} \\ & + 2s^2(x-M)\frac{du_m}{dx} - (x-M)^2u_m \\ & -\alpha\Big\{ s\left[(x-M)^2+\frac{1}{2}\right]\frac{d}{dx}(u_{m+1}-u_{m-1}) \\ & + s(x-M)\frac{d}{dx}(u_{m+1}+u_{m-1}) \\ & + s(x-M)(u_{m+1}-u_{m-1}) - \frac{1}{2}(u_{m+1}+u_{m-1}) - d_m u_m\Big\} \\ & -\frac{\alpha^2}{2}\Big\{[(x-M)^2+1]\left[u_m - \frac{1}{2}(u_{m+2}+u_{m-2})\right] \\ & - (x-M)(u_{m+2}-u_{m-2})\Big\}\Big\}, \end{aligned} \tag{1}$$

and the surface and vacuum energy can be written as

$$\begin{aligned}\delta W_{sv} = -\frac{2\pi^2}{nRq}\sum_m u_m^*(\Delta-M)\Big\{ & s(x-M)\frac{d}{dx}u_m \\ & + [2-(\Delta-M)]u_m \\ & -\frac{\alpha}{2}(\Delta-M)(u_{m+1}-u_{m-1})\Big\}_{x=\Delta}, \end{aligned} \tag{2}$$

where u_m is the mth Fourier components of the perturbations, m is the poloidal mode number, with m_0 being the one resonating at the first resonance surface at plasma edge, $M \equiv m_0 - m$, d_m is introduced to specify the magnetic well, and γ is the normalized growth rate, which is assumed to be very small for marginal stability investigation and used to eliminate the singularities near the resonance surfaces for numerical computation. Here, the coordinate system is shown in Fig. 1, $x \equiv m_0 - nq$, and Δ indicates plasma-vacuum interface. As usual we cut off the Fourier components beyond the minimum $M_{\min}$ and maximum $M_{\max}$ numbers. Total number of Fourier components is given by $N_g = M_{\max} - M_{\min} + 1$.

The Euler equations of Eq. (1) with inertial energy included are given as follows:[5]

$$\frac{d}{dx}\left(\mathcal{F}_{mm'}\frac{du_{m'}}{dx} + \mathcal{K}_{mm'}u_{m'}\right) - (\mathcal{K}^\dagger_{mm'}u'_{m'} + \mathcal{G}_{mm'}u_{m'}) = 0, \tag{3}$$

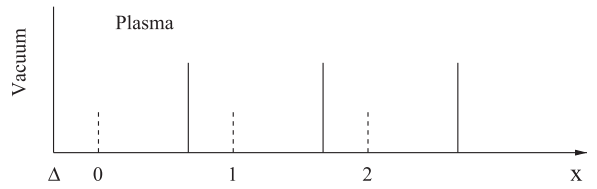

FIG. 1. Coordinate system, in which the vertical dashed lines represent the resonance surfaces and the vertical solid lines denote the region boundaries.

where

$$\mathcal{F}_{mm'} = \begin{cases} s^2[(x-M)^2-\omega^2], & \text{for} \quad m'=m; \\ 0, \quad \text{otherwise}; \end{cases} \tag{4}$$

$$\mathcal{K}_{mm'} = \begin{cases} \mp(\alpha s/2)(x-M)(x-M\pm1)\mp\alpha s/4, & \text{for} \quad m'=m\pm1; \\ 0, \quad \text{otherwise}; \end{cases} \tag{5}$$

$$\mathcal{G}_{mm'} = \begin{cases} (x-M)^2-\alpha d_m+(\alpha^2/2)[(x-M)^2+1], & \text{for } m'=m; \\ -\alpha/2(1+s), & \text{for } m'=m\pm1; \\ -(\alpha^2/4)(x-M\pm1)^2, & \text{for } m'=m\pm2; \\ 0, \quad \text{otherwise}. \end{cases} \tag{6}$$

In Eq. (3), the summation is assumed to be performed with respect to repeated indices, the prime on u_m denotes derivative with respect to x, and the superscript dagger represents Hermitian conjugation.

There are two set of boundary conditions for the coupled differential equation (3). As $x \to +\infty$, it is required that $u_m x \to 0$, for all m. At the plasma-vacuum interface, the variation of the surface-vacuum energy in Eq. (2) leads to the following conditions:[5]

$$\mathcal{F}_{mm'}\frac{du_{m'}}{dx} + \mathcal{K}_{mm'}u_{m'} - \mathcal{V}_{mm'}u_{m'} = 0. \tag{7}$$

This condition can be used to determine the eigenmodes and eigenvalues.

III. INTERNAL BALLOONING MODE REPRESENTATION IN CONFIGURATION SPACE

Before introducing the free boundary ballooning mode representation, we first outline the internal ballooning mode representation in the configuration space. This configuration-space representation is an analogue to the conventional one and is presented to explain the independent solution method for including the invariance properties.

The eigenvalue problem in Eq. (3) is a 2D problem, which involves N poloidal Fourier components in the radial space: $-\infty < x < \infty$. For high n modes, the distance between nearby mode rational surfaces is much smaller than the equilibrium scale length. Therefore, the Fourier components of the perturbation exhibit a translational invariance in the lowest order, as shown in Fig. 2. Mathematically, this invariance can be expressed as[1–3]

$$u_m(x \pm k) = u_{m\pm k}(x)\exp\{\mp ik\theta_k\}. \tag{8}$$

In the conventional ballooning formalism, this invariance is used to express the sidebands with the main harmonic with suitable spatial shifts. Consequently, Eq. (3) is transformed into an equation for a single Fourier component. This procedure reduces the 2D problem to 1D one by eliminating the poloidal dimension.

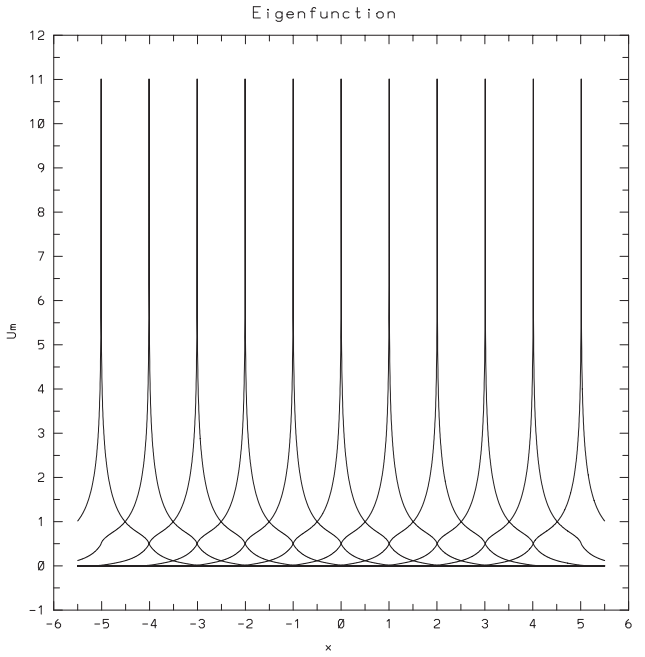

FIG. 2. Invariant structure of the high n internal ballooning modes.

Alternatively, we can use the invariance in Eq. (8) to reduce the radial dimension from the infinite domain to a single interval: $\Delta < x < 1 + \Delta$. One can solve the eigenmode equation (3) for all Fourier components in a single interval

$$\Delta < x < 1 + \Delta, \tag{9}$$

and then derive the solutions in other intervals by applying the translational invariance in Eq. (8). For this single interval the ballooning mode representation in Eq. (8) can be used to construct the boundary conditions for the N Fourier components

$$u_m(1+\Delta) = e^{-i\theta_k} u_{m+1}(\Delta), \tag{10}$$

$$\frac{d}{dx} u_m(1+\Delta) = e^{-i\theta_k} \frac{d}{dx} u_{m+1}(\Delta). \tag{11}$$

Note that for farthest sidebands ($m_{\min}$ and $m_{\max}$), one can require

$$u_{m_{\max}}(1+\Delta) = 0, \tag{12}$$

$$u_{m_{\min}}(\Delta) = 0. \tag{13}$$

Here, in principle, the small asymptotic solutions should be used as the boundary conditions for farthest sidebands. But, when sufficient number of sidebands are used, the boundary conditions in Eqs. (12) and (13) are good enough. Note that the conditions in Eqs. (10)–(13) completely determine the all Fourier components in the interval in Eq. (9) with eigen frequency. This also reduces the 2D problem to an 1D one.

To explain the equivalence of the current formalism to the conventional one, let us use the independent solution method to solve Eq. (3) in a single interval with the boundary conditions in Eqs. (10)–(13) imposed. We cut off the Fourier components beyond the minimum $m_{\min}$ and maximum $m_{\max}$ numbers in this interval. Total number of Fourier components for describing this interval is then given by $N = m_{\max} - m_{\min} + 1$. Note that Eq. (3) are a set of second order differential equations. They can be transformed to a set of first order differential equations for 2 N unknowns y_m, as specified as follows:

$$\begin{aligned} y_1 &= u_{m_{\max}}, \\ y_2 &= \frac{d}{dx} u_{m_{\max}}, \\ &\vdots \\ y_{2N-1} &= u_{m_{\min}}, \\ y_{2N} &= \frac{d}{dx} u_{m_{\min}}. \end{aligned} \tag{14}$$

We introduce bold face to denote the corresponding $2N$ component vector, for example $\mathbf{y}$ for $\{y_m\}$. Equation (3) with boundary condition, Eq. (12) imposed allows $2N-1$ independent solutions ${}^j\mathbf{y}\,(j = 1, \cdots, 2N-1)$. The independent solutions ${}^j\mathbf{y}$ for Eq. (3) can be obtained by shooting code from $\Delta + 1$ to Δ, with the following $2N-1$ initial conditions at $x = 1 + \Delta$ imposed:

$$\{{}^1\mathbf{y}, {}^2\mathbf{y}, \cdots, {}^{2N-1}\mathbf{y}\}_{x=1+\Delta} = \begin{pmatrix} 0^{1\times(2N-1)} \\ \mathcal{I}^{(2N-1)\times(2N-1)} \end{pmatrix}, \tag{15}$$

where $0^{1\times(2N-1)}$ and $\mathcal{I}^{(2N-1)\times(2N-1)}$ are respectively the zero and unitary matrices with dimensions indicated by their superscripts. The general solution can therefore be expressed as

$$\mathbf{y} = \{{}^1\mathbf{y}, {}^2\mathbf{y}, \cdots, {}^{2N-1}\mathbf{y}\} \cdot \mathbf{c}, \tag{16}$$

where $\mathbf{c}$ is the constant vector of $2N-1$ components, which are determined by the boundary conditions.

To construct the eigenvalue problem, we introduce following two square $(2N-1) \times (2N-1)$ matrices, which consist of the values of independent solutions at both ends of the interval,

$$\mathcal{L} \equiv \begin{pmatrix} {}^1y_1 & {}^2y_1 & \cdots & {}^{2N-1}y_1 \\ {}^1y_2 & {}^2y_2 & \cdots & {}^{2N-1}y_2 \\ \vdots & \vdots & \cdots & \vdots \\ {}^1y_{2N-3} & {}^2y_{2N-3} & \cdots & {}^{2N-1}y_{2N-3} \\ {}^1y_{2N-2} & {}^2y_{2N-2} & \cdots & {}^{2N-1}y_{2N-2} \\ {}^1y_{2N-1} & {}^2y_{2N-1} & \cdots & {}^{2N-1}y_{2N-1} \end{pmatrix}_{x=\Delta}, \tag{17}$$

$$\begin{aligned} \mathcal{R} &\equiv \begin{pmatrix} {}^1y_3 & {}^2y_3 & \cdots & {}^{2N-1}y_3 \\ {}^1y_4 & {}^2y_4 & \cdots & {}^{2N-1}y_4 \\ \vdots & \vdots & \cdots & \vdots \\ {}^1y_{2N-1} & {}^2y_{2N-1} & \cdots & {}^{2N-1}y_{2N-1} \\ {}^1y_{2N} & {}^2y_{2N} & \cdots & {}^{2N-1}y_{2N} \\ 0 & 0 & \cdots & 0 \end{pmatrix}_{x=1+\Delta} \\ &= \begin{pmatrix} 0 & 1 & \cdots & 0 & 0 \\ 0 & 0 & \cdots & 0 & 0 \\ \vdots & \vdots & \cdots & \vdots & \vdots \\ 0 & 0 & \cdots & 1 & 0 \\ 0 & 0 & \cdots & 0 & 1 \\ 0 & 0 & \cdots & 0 & 0 \end{pmatrix}. \end{aligned} \tag{18}$$

Here, in the definition of matrix $\mathcal{R}$ we have used the boundary conditions in Eq. (15). Note that the boundary condition in Eq. (12) has been taken into account in constructing the independent solutions in Eq. (15). The rest conditions in Eqs. (10), (11), and (13) can be used to determine the constant vector **c** as follows:

$$(\mathcal{R} - e^{-i\theta_k}\mathcal{L}) \cdot \mathbf{c} = 0, \tag{19}$$

where θ_k is the usual ballooning mode phase. The last row of this equation is derived from Eq. (13), and the rest from Eqs. (10) and (11). The existence of non-vanishing solutions for Eq. (19) gives the following dispersion relation:

$$\det|\mathcal{R} - e^{-i\theta_k}\mathcal{L}| = 0. \tag{20}$$

Equation (20) can be used to determine the eigen growth rate, so that the stability condition can be obtained. As a numerical example, Fig. 3 shows the marginal stable eigen modes in the interval $-0.5 < x < 0.5$ for the case with $\theta_k = 0$, $s = 0.4$, $\alpha = 0.3546$, and $d_m = 0$. The critical beta value agrees completely with the conventional ballooning mode theory.[1,11] One can spread out the sidebands from the interval $-0.5 < x < 0.5$ to other intervals according to the ballooning invariance in Eq. (8). The expanded figure is given in Fig. 4. This is exactly the single Fourier component in whole ballooning Fourier spectrum as shown in Fig. 2. The smooth connection of the expanded figure is assured by the boundary conditions in Eqs. (10) and (11). This example shows how the 2D problem (multiple Fourier components) can be transformed into a 1D problem by a reduction in the radial direction. The computation resource used for computing multiple Fourier components in a single interval is equivalent to that for a single Fourier component in the expanded space. Therefore, the current method uses the same amount of computation resource as the conventional approach.

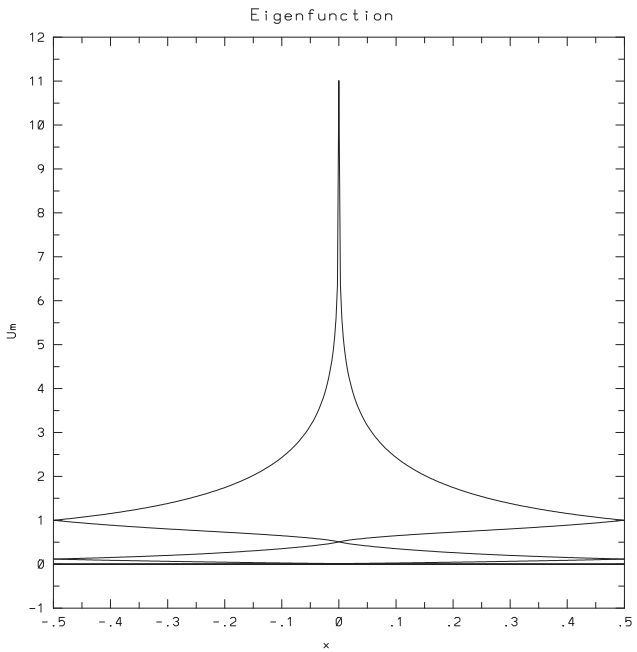

FIG. 3. Internal ballooning eigenmode as computed in a single interval, using the conventional ballooning mode representation for boundary conditions with $\theta_k = 0$. The equilibrium parameters are as follows: $s = 0.4$, $\alpha = 0.3546$, and $d_m = 0$.

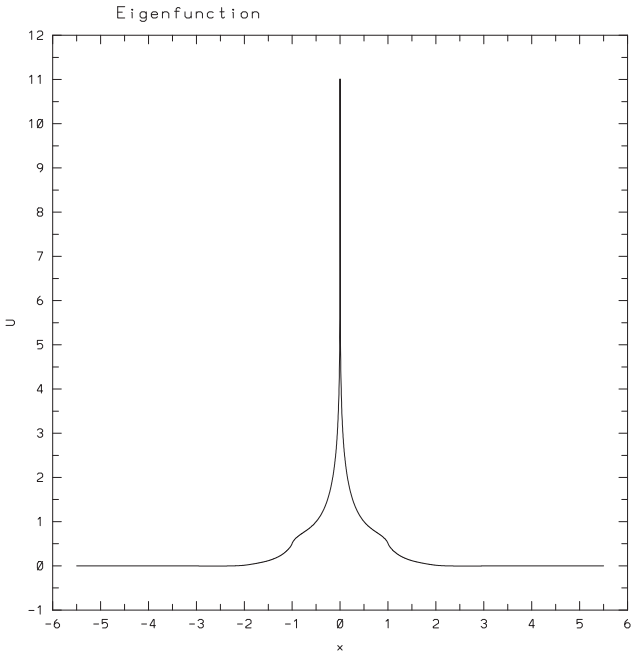

FIG. 4. Single Fourier component obtained by spreading out the sidebands ($m \neq m_0$) in Fig. 3 to the expanded radial space according to the ballooning invariance in Eq. (8).

In this section, we discuss only the lowest order solution. The conventional theory for next order correction, for example in Ref. 1, can be applicable here. This issue will be further discussed in Sec. V.

IV. FREE BOUNDARY BALLOONING MODE REPRESENTATION

In the plasma edge region, the conventional ballooning mode invariance becomes no more valid. Nevertheless, as shown in this section, there is a more fundamental invariance that can be used to reduce the 2D problem of external high n modes to a 1D one. To help understand the formalism described below, we include the Appendix to delineate the underlying thoughts in a reduced model. To discuss the free boundary ballooning representation we consider the lowest order solution, i.e., neglecting the radial variance of equilibrium quantities. The next order correction will be studied in Sec. V.

We need to discuss the free boundary ballooning modes with all intervals involved. The system to be considered is shown in Fig. 1. The intervals are labeled from "1" to "$k_{\max}$" from the one adjacent to plasma vacuum interface to the farthest one in the plasma core. The kth region is thus defined as

$$\Delta + k - 1 < x < \Delta + k, \qquad k = 1, 2, \cdots, k_{\max}. \tag{21}$$

For specificity, we assume that the safety factor increases monotonically from plasma core to edge. In the high n mode case, the distance between intervals is very small as compared to the equilibrium scale length. Therefore, the equilibrium quantities can be regarded to be unchanged in the

lowest order. The resonant Fourier component in the kth regions is denoted as ${}^{k}m_0$, with ${}^{1}m_0 \equiv m_0$. One then has ${}^{k}m_0 = m_0 - k + 1$. Due to the equilibrium similarity of each interval, we can use the same number of Fourier components (N) to describe each interval. Denoting the lower and upper cutting-off Fourier components for kth region as ${}^{k}m_{\min}$ and ${}^{k}m_{\max}$, with ${}^{1}m_{\min} \equiv m_{\min}$ and ${}^{1}m_{\max} \equiv m_{\max}$, one has ${}^{k}m_{\min} = m_{\min} - k + 1$ and ${}^{k}m_{\max} = m_{\max} - k + 1$. The total number of Fourier components in a interval becomes $N = m_{\max} - m_{\min} + 1$. We require the farthest sidebands in the kth interval to vanish

$$u_{{}^{k}m_{\min}}(\Delta + k - 1) = 0, \tag{22}$$

$$u_{{}^{k}m_{\max}}(\Delta + k) = 0. \tag{23}$$

Similar to Eq. (14), we denote the $2N$ unknowns in the kth interval as

$$\begin{aligned} y_1 &= u_{{}^{k}m_{\max}}, \\ y_2 &= \frac{d}{dx} u_{{}^{k}m_{\max}}, \\ &\vdots \\ y_{2N-1} &= u_{{}^{k}m_{\min}}, \\ y_{2N} &= \frac{d}{dx} u_{{}^{k}m_{\min}}. \end{aligned} \tag{24}$$

We can construct the independent solutions in each interval in the same way by imposing the boundary conditions at the respective right ends. The independent solutions for kth interval ${}^{j}\mathbf{y}$ can be found by shooting code from $\Delta + k$ to $\Delta + k - 1$, with the following $2N - 1$ initial conditions at $x = \Delta + k$ imposed

$$\{{}^{1}\mathbf{y}, {}^{2}\mathbf{y}, \cdots, {}^{2N-1}\mathbf{y}\}_{x=\Delta+k} = \begin{pmatrix} 0^{1\times(2N-1)} \\ \mathcal{I}^{(2N-1)\times(2N-1)} \end{pmatrix}. \tag{25}$$

The general solution in the kth region can be expressed as

$$\mathbf{y}(x) = {}^{k}\mathcal{Y} \cdot {}^{k}\mathbf{c} = \{{}^{1}\mathbf{y}, {}^{2}\mathbf{y}, \cdots, {}^{2N-1}\mathbf{y}\} \cdot {}^{k}\mathbf{c}, \tag{26}$$

where ${}^{k}\mathbf{c}$ are constant vectors, which are determined by the boundary conditions and matching conditions between intervals. From the analysis in Sec. III, one can see that the conventional ballooning invariance requires both independent solutions and boundary conditions to be invariant. The requirement for boundary part makes the conventional ballooning mode representation inapplicable for edge region. Actually, the requirements for boundary value invariance are unnecessary. The invariance of independent solutions is more fundamental. Mathematically, this invariance can be expressed as follows:

$${}^{j}u_{m \mp 2k}(x \pm k) = {}^{j}u_m(x), \tag{27}$$

where j labels the independent solutions. The difference from the conventional ballooning invariance in Eq. (8) lies in that the invariance here is related to the independent solutions, instead of the Fourier components of the perturbation. When the independent solutions are obtained in a single interval, one actually obtains the independent solutions in all intervals by applying the invariance in Eq. (27). With the independent solutions known for all intervals, the eigenvalue problem can be constructed through fitting the continuity conditions between intervals and boundary conditions at the plasma core and vacuum-plasma interface.

Let us describe the detailed procedure. First, we use the shooting code to obtain the independent solutions in the first interval, using Eq. (25) as initial conditions at the right end. To construct the eigenvalue problem, we define the following two square $(2N-1) \times (2N-1)$ matrices, which consist of the values of independent solutions at the kth interval boundaries

$$\begin{aligned} \mathcal{L} &\equiv \begin{pmatrix} {}^{1}y_1 & {}^{2}y_1 & \cdots & {}^{2N-1}y_1 \\ {}^{1}y_2 & {}^{2}y_2 & \cdots & {}^{2N-1}y_2 \\ \vdots & \vdots & \cdots & \vdots \\ {}^{1}y_{2N-3} & {}^{2}y_{2N-3} & \cdots & {}^{2N-1}y_{2N-3} \\ {}^{1}y_{2N-2} & {}^{2}y_{2N-2} & \cdots & {}^{2N-1}y_{2N-2} \\ {}^{1}y_{2N-1} & {}^{2}y_{2N-1} & \cdots & {}^{2N-1}y_{2N-1} \end{pmatrix}_{x=\Delta+k-1}, \\ \mathcal{R} &\equiv \begin{pmatrix} {}^{1}y_3 & {}^{2}y_3 & \cdots & {}^{2N-1}y_3 \\ {}^{1}y_4 & {}^{2}y_4 & \cdots & {}^{2N-1}y_4 \\ \vdots & \vdots & \cdots & \vdots \\ {}^{1}y_{2N-1} & {}^{2}y_{2N-1} & \cdots & {}^{2N-1}y_{2N-1} \\ {}^{1}y_{2N} & {}^{2}y_{2N} & \cdots & {}^{2N-1}y_{2N} \\ 0 & 0 & \cdots & 0 \end{pmatrix}_{x=\Delta+k} \\ &= \begin{pmatrix} 0 & 1 & \cdots & 0 & 0 \\ 0 & 0 & \cdots & 0 & 0 \\ \vdots & \vdots & \cdots & \vdots & \vdots \\ 0 & 0 & \cdots & 1 & 0 \\ 0 & 0 & \cdots & 0 & 1 \\ 0 & 0 & \cdots & 0 & 0 \end{pmatrix}. \end{aligned} \tag{28}$$

We also introduce the following $(2N-1) \times N$ matrix for the last interval

$${}^{k_{\max}}\mathcal{L} \equiv \begin{pmatrix} {}^{1}y_1 & {}^{3}y_1 & \cdots & {}^{2N-3}y_1 & {}^{2N-1}y_1 \\ {}^{1}y_2 & {}^{3}y_2 & \cdots & {}^{2N-3}y_2 & {}^{2N-1}y_2 \\ \vdots & \vdots & \cdots & \vdots & \vdots \\ {}^{1}y_{2N-3} & {}^{3}y_{2N-3} & \cdots & {}^{2N-3}y_{2N-3} & {}^{2N-1}y_{2N-3} \\ {}^{1}y_{2N-2} & {}^{3}y_{2N-2} & \cdots & {}^{2N-3}y_{2N-2} & {}^{2N-1}y_{2N-2} \\ {}^{1}y_{2N-1} & {}^{3}y_{2N-1} & \cdots & {}^{2N-3}y_{2N-1} & {}^{2N-1}y_{2N-1} \end{pmatrix}_{x=\Delta+k_{\max}-1}. \tag{29}$$

Due to the invariance property in Eq. (27), the matrices $\mathcal{L}$ (including ${}^{k_{\max}}\mathcal{L}$) and $\mathcal{R}$ in Eqs. (28) and (29) are interval-independent. Therefore, we can construct $\mathcal{L}$ (including ${}^{k_{\max}}\mathcal{L}$) and $\mathcal{R}$ with the independent solutions in the first interval, i.e., we can substitute the subscripts on the right hand sides of Eqs. (28) and (29): $x = \Delta + k - 1$, $x = \Delta + k$, and $x = \Delta + k_{\max} - 1$ with $x = \Delta$, $x = \Delta + 1$, and $x = \Delta$, respectively.

Next, let us deal with the boundary conditions at the core plasma and the matching conditions between intervals. Note that the matrix ${}^{k_{\max}}\mathcal{L}$ in Eq. (29) picks up only the independent solutions that satisfy the boundary conditions ${}^{j}\mathbf{y} = 0$

at the farthest end in the plasma core. Therefore, the replacement of $\mathcal{L}$ with ${}^{k_{\max}}\mathcal{L}$ at the last interval can guarantee the satisfaction of the boundary condition $\mathbf{y}=0$ at the innermost side toward plasma core. Therefore, using ${}^{k}\mathbf{c}$ to construct the general solutions as in Eq. (26), there are only number N independent solutions left for the $k_{\max}$ interval, while for the rest of intervals there remain number $2N-1$ independent solutions. The matching conditions between the $k_{\max}$ and $k_{\max-1}$ intervals becomes

$$ {}^{k_{\max}}\mathcal{L}\cdot{}^{k_{\max}}\mathbf{c}=\mathcal{R}\cdot{}^{k_{\max}-1}\mathbf{c}. \tag{30}$$

and the matching conditions between k and $k+1$ (with $k=1,\cdots,k_{\max}-2$) intervals are

$$ \mathcal{L}\cdot{}^{k+1}\mathbf{c}=\mathcal{R}\cdot{}^{k}\mathbf{c}. \tag{31}$$

Equations (30) and (31) can be expressed as matrix form

$$\begin{pmatrix} {}^{k_{\max}}\mathcal{L}^{(2N-1)\times N} & -\mathcal{R}^{(2N-1)\times(2N-1)} & 0^{(2N-1)\times(2N-1)} & \cdots & 0^{(2N-1)\times(2N-1)} & 0^{(2N-1)\times(2N-1)} \\ 0^{(2N-1)\times N} & \mathcal{L}^{(2N-1)\times(2N-1)} & -\mathcal{R}^{(2N-1)\times(2N-1)} & \cdots & 0^{(2N-1)\times(2N-1)} & 0^{(2N-1)\times(2N-1)} \\ \vdots & \vdots & \vdots & \cdots & \vdots & \vdots \\ 0^{(2N-1)\times N} & 0^{(2N-1)\times(2N-1)} & 0^{(2N-1)\times(2N-1)} & \cdots & \mathcal{L}^{(2N-1)\times(2N-1)} & -\mathcal{R}^{(2N-1)\times(2N-1)} \end{pmatrix} \times \begin{pmatrix} {}^{k_{\max}}\mathbf{c}^{N\times 1} \\ {}^{k_{\max}-1}\mathbf{c}^{(2N-1)\times 1} \\ \vdots \\ {}^{1}\mathbf{c}^{(2N-1)\times 1} \end{pmatrix} = \begin{pmatrix} 0^{(2N-1)\times 1} \\ 0^{(2N-1)\times 1} \\ \vdots \\ 0^{(2N-1)\times 1} \end{pmatrix}, \tag{32}$$

where again the matrix dimensions are explicitly denoted by the respective right superscripts. Here, the number of linear equations is $(k_{\max}-1)(2N-1)$, while the number of unknowns ${}^{k}\mathbf{c}$ is $(k_{\max}-1)(2N-1)+N$. There are number N excessive unknowns. These excessive unknowns are required to fit the boundary conditions at the plasma-vacuum interface. To single out the N excessive unknowns, we introduce the following normalization procedure. Without losing generality, one can use the freedom of choosing the excessive N unknowns to define the normalization of independent solutions. We use for example the following normalization for global independent solutions at the plasma-vacuum interface:

$$ {}^{k}u_m|_{x=\Delta}=\delta_{km}, \tag{33}$$

where $\delta_{km}=1$ when $k=m$, otherwise $\delta_{km}=0$. Including the normalization conditions in Eq. (33) to define the excessive N unknowns, Eq. (32) is transformed to the following matrix equations

$$\begin{pmatrix} {}^{k_{\max}}\mathcal{L}^{(2N-1)\times N} & -\mathcal{R}^{(2N-1)\times(2N-1)} & 0^{(2N-1)\times(2N-1)} & \cdots & 0^{(2N-1)\times(2N-1)} & 0^{(2N-1)\times(2N-1)} \\ 0^{(2N-1)\times N} & \mathcal{L}^{(2N-1)\times(2N-1)} & -\mathcal{R}^{(2N-1)\times(2N-1)} & \cdots & 0^{(2N-1)\times(2N-1)} & 0^{(2N-1)\times(2N-1)} \\ \vdots & \vdots & \vdots & \cdots & \vdots & \vdots \\ 0^{(2N-1)\times N} & 0^{(2N-1)\times(2N-1)} & 0^{(2N-1)\times(2N-1)} & \cdots & \mathcal{L}^{(2N-1)\times(2N-1)} & -\mathcal{R}^{(2N-1)\times(2N-1)} \\ 0^{N\times N} & 0^{N\times(2N-1)} & 0^{N\times(2N-1)} & \cdots & 0^{N\times(2N-1)} & \mathcal{L}_o^{N\times(2N-1)} \end{pmatrix} \times \begin{pmatrix} {}^{k_{\max}}\mathcal{C}^{N\times N} \\ {}^{k_{\max}-1}\mathcal{C}^{(2N-1)\times N} \\ {}^{k_{\max}-2}\mathcal{C}^{(2N-1)\times N} \\ \vdots \\ {}^{1}\mathcal{C}^{(2N-1)\times N} \end{pmatrix} = \begin{pmatrix} 0^{(2N-1)\times N} \\ 0^{(2N-1)\times N} \\ \vdots \\ 0^{(2N-1)\times N} \\ \mathcal{I}^{N\times N} \end{pmatrix}, \tag{34}$$

where the $N\times(2N-1)$ matrix

$$\mathcal{L}_0\equiv\begin{pmatrix} {}^{1}y_1 & {}^{2}y_1 & \cdots & {}^{2N-1}y_1 \\ {}^{1}y_3 & {}^{2}y_3 & \cdots & {}^{2N-1}y_3 \\ \vdots & \vdots & \cdots & \vdots \\ {}^{1}y_{2N-3} & {}^{2}y_{2N-3} & \cdots & {}^{2N-1}y_{2N-3} \\ {}^{1}y_{2N-1} & {}^{2}y_{2N-1} & \cdots & {}^{2N-1}y_{2N-1} \end{pmatrix}_{x=\Delta}. \tag{35}$$

Here, $\mathcal{L}_0$ is constructed according to the normalization condition in Eq. (33).

The solution of Eq. (34), $\{{}^{k}\mathcal{C}\}$, can be found directly by the matrix inversion procedure or formally by the following recurrence relations

$$ {}^{k_{\max}-1}\mathcal{C}=\mathcal{R}^{-1}\ {}^{k_{\max}}\mathcal{L}\ {}^{k_{\max}}\mathcal{C}, \tag{36}$$

$$ {}^{k}\mathcal{C} = (\mathcal{R}^{-1}\mathcal{L})^{k_{\max}-k-1}\ \mathcal{R}^{-1}{}^{k_{\max}}\mathcal{L}\ {}^{k_{\max}}\mathcal{C}, \quad \text{for } k = 1, \cdots, k_{\max}-2, \tag{37} $$

$$ {}^{k_{\max}}\mathcal{C} = [\mathcal{L}_0(\mathcal{R}^{-1}\mathcal{L})^{k_{\max}-2}\ \mathcal{R}^{-1}{}^{k_{\max}}\mathcal{L}]^{-1}. \tag{38} $$

Here, Eq. (36) is obtained from the first row of Eq. (34), Eq. (37) from the second to the last but one row, and Eq. (38) from the last row with ${}^{1}\mathcal{C}$ from Eq. (37). When ${}^{k_{\max}}\mathcal{C}$ is determined using $\mathcal{R}$ and various $\mathcal{L}$'s by Eq. (38), the rest ${}^{k}\mathcal{C}$ can be evaluated by Eqs. (36) and (37).

Each of the N columns of solution matrix $\{{}^{k}\mathcal{C}\}$ can be used to construct a set of solutions in every intervals according to Eq. (26). The number N columns generate number N sets of solutions. These N sets of solutions over every interval can be connected respectively to form number N global independent solutions over the whole domain ${}^{j}\mathbf{y}_g\ (j = 1, \cdots, N)$, which satisfy the boundary conditions ${}^{j}\mathbf{y}_g = 0$ at $x \to \infty$, the normalization conditions in Eq. (33), and the continuity conditions between intervals. The general global solution is the linear combination of these N global independent solutions

$$ \mathbf{y}^{2N} = \mathcal{Y}^{2N\times N} \cdot \mathbf{c}_g^N = \{{}^{1}\mathbf{y}_g, \cdots, {}^{N}\mathbf{y}_g\}^{2N\times N} \cdot \mathbf{c}_g^N. \tag{39} $$

Here, the right superscripts are used to indicate the matrix dimensions.

Now, we can consider the boundary condition Eq. (7) at the plasma-vacuum interface to construct the eigenvalue problem. From Eq. (24), we can find the relationship between the ordinal number m for Fourier components and the matrix index i: $m = m_{\max} - (i-1)/2$ for $i = 1, 3, \cdots$. Therefore, using Eq. (39), the boundary condition Eq. (7) becomes

$$ \mathcal{D} \cdot \mathbf{c}_g = 0, \tag{40} $$

where the elements of $N \times N$ matrix $\mathcal{D}$ are given as follows:

$$ \begin{aligned} D_{ij} = {} & [\Delta - (i_0 - i)]\{-s[\Delta - (i_0 - i)]\mathcal{Y}_{2i,j} \\ & -[2 - [\Delta - (i_0 - i)]]\mathcal{Y}_{2(i-1)+1,j} \\ & +\frac{\alpha}{2}[\Delta - (i_0 - i)](\mathcal{Y}_{2(i-2)+1,j} - \mathcal{Y}_{2i+1,j})\}. \end{aligned} \tag{41} $$

Here, $i_0 = m_0 - m_{\max} + 1$, and $\mathcal{Y}_{-1,j} = \mathcal{Y}_{2M+1,j} = 0$. From Eq. (3), one can see that $\mathcal{D}$ is a function of the growth rate γ. The eigenvalue can be determined by

$$ \det|\mathcal{D}(\gamma)| = 0. \tag{42} $$

For marginal stability problem, one can choose a very small γ for shooting code to get independent solutions in the first interval in the plasma region. The stability is then simply determined by the eigenvalue problem[5]

$$ \mathcal{D} \cdot \mathbf{c}_g = \lambda \mathbf{c}_g. \tag{43} $$

If the eigenvalue $\lambda \geq 0$, the system is stable, otherwise unstable.

With the free ballooning mode formalism described above, we can now apply this formalism to determine the peel-ballooning eigenmode stability. The procedure is as follows: First, we construct the independent solutions in a single interval: $\Delta \leq x \leq \Delta + 1$, and use these independent solutions to construct matrices: $\mathcal{L}$, $\mathcal{R}$, ${}^{k_{\max}}\mathcal{L}$, and $\mathcal{L}_0$. Second, using these independent solution matrices, we can solve for $\{{}^{k}\mathcal{C}\}$ from Eq. (34) (or equivalently Eqs. (36)–(38)). With $\{{}^{k}\mathcal{C}\}$, one can construct the global independent solution matrix $\mathcal{Y}$ in Eq. (39). Thirdly, one can use the matrix $\mathcal{Y}$ to construct the eigenmatrix $\mathcal{D}$ in Eq. (41). Finally, one can determine the eigenvalue from Eq. (42) and eigenvectors from Eq. (40). The stability condition is determined by the eigenvalue. For the marginal stability problem, one can alternatively use Eq. (43) to determine the stability.

As numerical examples, we use this procedure to compute two cases in the s-α equilibrium model: The first is for the case with the resonance surface nearest to the plasma-vacuum interface residing in the plasma region, the second is for the case with the nearest resonance surface being in the vacuum region. Their parameters are, respectively, as follows: $s = 0.4$, $\alpha = 0.3$, $d_m = 0$, and $\Delta = -0.05$ for the first case; $s = 1.8$, $\alpha = 1.05$, $d_m = 0$, and $\Delta = -0.9$ for the second case. Both cases are ballooning mode stable. The maginal beta values for internal ballooning stability for the first case is $\alpha = 0.3546$, and for the second case is $\alpha = 1.0514$. We find peeling ballooning mode instabilities in both cases. Their eigenmodes are plotted in Figs. 5 and 6, respectively. We have compared these results with the 2D results by the AEGIS code (s-α version).[12] Completely agreements are found, in view of that in our equilibrium model the equilibrium parameters s, α, and d_m are constants.

Before proceeding to the next order theory in Sec. V, we note that the current lowest order theory satisfies both

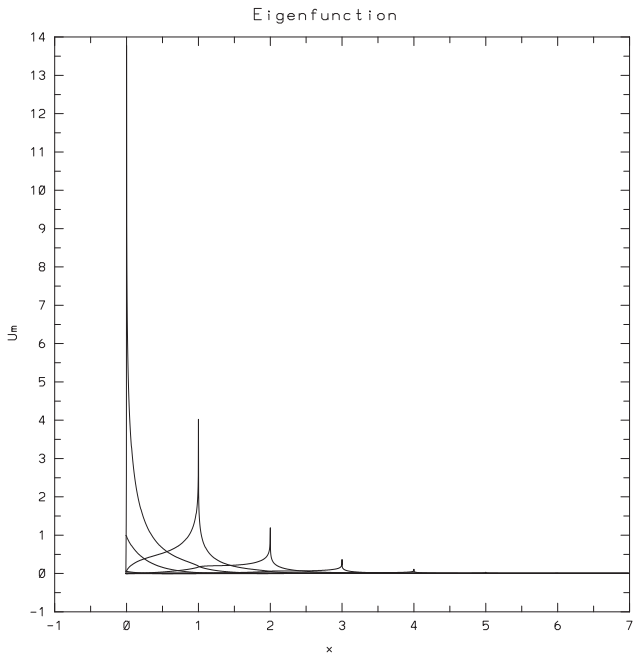

FIG. 5. Peeling-ballooning modes computed using the free boundary ballooning representation, with the nearest resonance surface being in the plasma region $\Delta = -0.05$. The equilibrium parameters are as follows: $s = 0.4$, $\alpha = 0.3$, and $d_m = 0$.

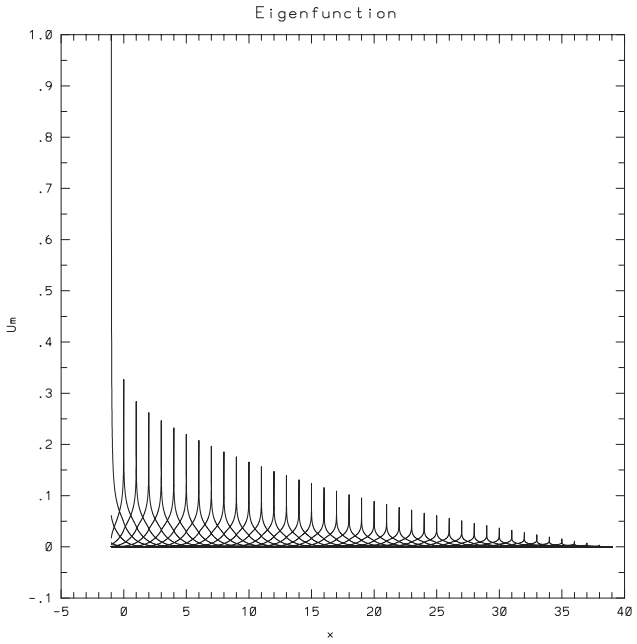

FIG. 6. Peeling-ballooning modes computed using the free boundary ballooning representation, with the nearest resonance surface being in the vacuum region $\Delta = -0.99$. The equilibrium parameters are as follows: $s = 1.8$, $\alpha = 1.05$, and $d_m = 0$.

the lowest order equations and boundary conditions. Therefore, the applicability of current lowest order theory is independent of the convergency of the next order solution. This is different from the conventional ballooning mode theory, in which the lowest order solution does not satisfy the global radial boundary conditions (see Fig. 2). The applicability of the lowest order theory in the conventional ballooning theory depends therefore on the convergence of next order solution in order to get an overall profile that satisfies the global boundary conditions (see for example Refs. 1 and 5).

V. FIRST ORDER SOLUTION FOR FREE BOUNDARY BALLOONING MODE THEORY

In this section, we investigate the next order theory. This is the first order correction to the lowest order theory presented in the last section. The conventional theory for next order correction in Ref. 5 does not apply here. This is because the theory in Ref. 5 relies on the assumption that the lowest order solutions are of the small type at the singular layers (see also the further discussion in the last section). This does not characterize the peeling component in our lowest order theory.

To derive the next order equation, the perturbed quantities are expanded as follows:

$$u_m = u_m + \delta u_m. \tag{44}$$

We have denoted the perturbed quantities with tag "δ" and used the same letters for both lowest and full quantities. Similarly, the equilibrium matrices are expanded as

$$\mathcal{F}_{mm'} = \mathcal{F}_{mm'} + \delta\mathcal{F}_{mm'} + \frac{\partial \mathcal{F}_{mm'}}{\partial \gamma}\delta\gamma, \tag{45}$$

$$\mathcal{K}_{mm'} = \mathcal{K}_{mm'} + \delta\mathcal{K}_{mm'}, \tag{46}$$

$$\mathcal{G}_{mm'} = \mathcal{G}_{mm'} + \delta\mathcal{G}_{mm'}, \tag{47}$$

where $\delta\mathcal{F}_{mm'} = \mathcal{F}_{mm'} - \langle \mathcal{F}_{mm'} \rangle_r$, with $\langle \cdots \rangle_r$ denoting the average over entire radial domain to be considered. As defined in Eqs. (4)–(6) we assume that only matrix $\mathcal{F}_{mm'}$ depends on the eigen growth rate γ. Note that the Euler-Lagrange equation (3) is generic for MHD description.[13] The definitions of equilibrium matrices in Eqs. (4)–(6) can be extended beyond the lowest order expressions in $1/n$. Depending on the specific equilibrium, the order $\delta u_m/u_m$ can be chosen to be $1/n$ or its fractional power.

The next order equation can be then expressed as

$$\begin{aligned}
&\frac{d}{dx}\left(\mathcal{F}_{mm'}\frac{d\delta u_{m'}}{dx} + \mathcal{K}_{mm'}\delta u_{m'}\right) - \left(\mathcal{K}^{\dagger}_{mm'}\delta u'_{m'} + \mathcal{G}_{mm'}\delta u_{m'}\right) \\
&+\frac{d}{dx}\left(\delta\mathcal{F}_{mm'}\frac{du_{m'}}{dx} + \delta\mathcal{K}_{mm'}u_{m'}\right) - \left(\delta\mathcal{K}^{\dagger}_{mm'}u'_{m'} + \delta\mathcal{G}_{mm'}u_{m'}\right) \\
&+\delta\gamma\frac{d}{dx}\left(\frac{\partial\mathcal{F}_{mm'}}{\partial\gamma}\frac{du_{m'}}{dx}\right) = 0.
\end{aligned} \tag{48}$$

This is a set of inhomogeneous equations for unknowns δu_m. We can derive from Eq. (7) that the linearized boundary conditions for δu_m are as follows:

$$\begin{aligned}
&\left\{\mathcal{F}_{mm'}\frac{d\delta u_{m'}}{dx} + \mathcal{K}_{mm'}\delta u_{m'} - \mathcal{V}_{mm'}\delta u_{m'}\right. \\
&\quad+\left(\delta\mathcal{F}_{mm'} + \delta\gamma\frac{\partial\mathcal{F}}{\partial\gamma}\right)\frac{du_{m'}}{dx} + \delta\mathcal{K}_{mm'}u_{m'} \\
&\quad\left.-\delta\mathcal{V}_{mm'}u_{m'}\right\}_{x=\Delta} = 0,
\end{aligned} \tag{49}$$

$$\delta u_m|_{x\to+\infty} \to 0. \tag{50}$$

We can derive the next order correction of the eigen growth rate by applying the operator $\int_{\Delta}^{+\infty} u_m\{\cdots\}$ on Eq. (48). Using the boundary condition Eq. (49), the boundary conditions for u_m in Eq. (7), and the Hermitian property of the homogeneous part of Eq. (48), one can obtain

$$\delta\gamma = -\frac{\int_{\Delta}^{+\infty} dx[u'_m(\delta\mathcal{F}_{mm'}u'_{m'} + \delta\mathcal{K}_{mm'}u_{m'}) + u_m(\delta\mathcal{K}^{\dagger}_{mm'}u'_{m'} + \delta\mathcal{G}_{mm'}u_{m'})] + u_m\delta\mathcal{V}_{mm'}u_{m'}|_{\Delta}}{\int_{\Delta}^{+\infty} dx u'_m\frac{d\mathcal{F}_{mm'}}{d\gamma}u'_{m'}}. \tag{51}$$

Therefore, using the lowest order eigen function and lowest order eigen growth rate obtained in the last section we can compute the first order growth rate $\delta\gamma$ through Eq. (51). It is interesting to point out that, when the perturbed equilibrium quantities $\delta\mathcal{F}_{mm'}$, $\delta\mathcal{K}_{mm'}$, $\delta\mathcal{G}_{mm'}$, and $\delta\mathcal{V}_{mm'}$ vanish, the perturbed growth rate vanishes as well: $\delta\gamma = 0$. As discussed in the last section for the case with α and s being constant, this property is confirmed numerically by the global calculation.

Next, we derive the next order correction for eigenfunction. Equation (48) is a set of inhomogeneous equations for δu_m. Its solution is the sum of homogeneous solutions and special solutions. Note that the homogeneous part of Eq. (48) has the same structure as the lower order one investigated in the last section. Therefore, the same independent solutions can be used to construct the homogeneous solution of Eq. (48). As Eq. (26), the general solution of first order in the kth region can be expressed as

$$\delta\mathbf{y}(x) = \{{}^1\mathbf{y}, {}^2\mathbf{y}, \cdots, {}^{2N-1}\mathbf{y}\} \cdot {}^k\delta\mathbf{c} + {}^k\delta\mathbf{g}. \tag{52}$$

Here, ${}^k\delta\mathbf{g}$ denotes the special solution in the kth region. The special solution ${}^k\delta\mathbf{g}$ can be obtained by numerical shooting from $\Delta + k$ to $\Delta + k - 1$, with the initial condition ${}^k\delta\mathbf{g} = 0$ imposed at $x = \Delta + k$.

The constant vectors ${}^k\delta\mathbf{c}$ in Eq. (52) can be determined by the boundary and matching conditions. Note that the way constructing the special solution ${}^k\delta\mathbf{g}$ assures the boundary condition at $x \to +\infty$ in Eq. (50) to be satisfied. The boundary condition at plasma-vacuum interface Eq. (49) can be expressed as follows:

$$\mathcal{F}\mathcal{L}_d \cdot {}^1\delta\mathbf{c} + (\mathcal{K} - \mathcal{V})\mathcal{L}_0 \cdot {}^1\delta\mathbf{c} = \delta\mathbf{h}, \tag{53}$$

where

$$\delta\mathbf{h} = -\mathcal{F} \cdot {}^1\delta\mathbf{g}_d - (\mathcal{K} - \mathcal{V}) \cdot {}^1\delta\mathbf{g}_0 - \left(\delta\mathcal{F} + \delta\gamma \frac{\partial}{\partial\gamma}\mathcal{F}\right)\mathbf{u}' - (\delta\mathcal{K} - \delta\mathcal{V})\mathbf{u}$$

and $\mathbf{u}$ is a vector which is constituted by u_m. Here, $\mathcal{L}_0$ is defined in Eq. (35) and

$$\mathcal{L}_d \equiv \begin{pmatrix} {}^1y_2 & {}^2y_2 & \cdots & {}^{2N-1}y_2 \\ {}^1y_4 & {}^2y_4 & \cdots & {}^{2N-1}y_4 \\ \vdots & \vdots & \cdots & \vdots \\ {}^1y_{2N-2} & {}^2y_{2N-2} & \cdots & {}^{2N-1}y_{2N-2} \\ {}^1y_{2N} & {}^2y_{2N} & \cdots & {}^{2N-1}y_{2N} \end{pmatrix}_{x=\Delta},$$

$${}^1\delta\mathbf{g}_0 = \begin{pmatrix} {}^1\delta g_1 \\ {}^1\delta g_3 \\ \vdots \\ {}^1\delta g_{2N-1} \end{pmatrix}_{x=\Delta}, \qquad {}^1\delta\mathbf{g}_d = \begin{pmatrix} {}^1\delta g_2 \\ {}^1\delta g_4 \\ \vdots \\ {}^1\delta\mathbf{g}_{2N} \end{pmatrix}_{x=\Delta}.$$

The matching conditions between the last two neighboring regions $k_{\max} - 1$ and $k_{\max}$ can be expressed as follows:

$${}^{k_{\max}}\mathcal{L} \cdot {}^{k_{\max}}\delta\mathbf{c} + {}^{k_{\max}}\delta\mathbf{g} = \mathcal{R} \cdot {}^{k_{\max}-1}\delta\mathbf{c}. \tag{54}$$

The matching conditions between k and $k + 1$ regions are

$$\mathcal{L} \cdot {}^{k+1}\delta\mathbf{c} + {}^{k+1}\delta\mathbf{g} = \mathcal{R} \cdot {}^k\delta\mathbf{c}, \tag{55}$$

where $k = 1, \cdots, k_{\max} - 2$. The boundary and matching conditions in Eqs. (53)–(55) can be summarized in the following matrix equation:

$$\begin{pmatrix} {}^{k_{\max}}\mathcal{L}^{(2N-1)\times N} & -\mathcal{R}^{(2N-1)\times(2N-1)} & 0^{(2N-1)\times(2N-1)} & \cdots & 0^{(2N-1)\times(2N-1)} & 0^{(2N-1)\times(2N-1)} \\ 0^{(2N-1)\times N} & \mathcal{L}^{(2N-1)\times(2N-1)} & -\mathcal{R}^{(2N-1)\times(2N-1)} & \cdots & 0^{(2N-1)\times(2N-1)} & 0^{(2N-1)\times(2N-1)} \\ \vdots & \vdots & \vdots & \cdots & \vdots & \vdots \\ 0^{(2N-1)\times N} & 0^{(2N-1)\times(2N-1)} & 0^{(2N-1)\times(2N-1)} & \cdots & \mathcal{L}^{(2N-1)\times(2N-1)} & -\mathcal{R}^{(2N-1)\times(2N-1)} \\ 0^{N\times N} & 0^{N\times(2N-1)} & 0^{N\times(2N-1)} & \cdots & 0^{N\times(2N-1)} & [\mathcal{F}\mathcal{L}_d + (\mathcal{K} - \mathcal{V})\mathcal{L}_0]^{N\times(2N-1)} \end{pmatrix}$$

$$\times \begin{pmatrix} {}^{k_{\max}}\delta\mathbf{c}^{N\times 1} \\ {}^{k_{\max}-1}\delta\mathbf{c}^{(2N-1)\times 1} \\ {}^{k_{\max}-2}\delta\mathbf{c}^{(2N-1)\times 1} \\ \vdots \\ {}^1\delta\mathbf{c}^{(2N-1)\times 1} \end{pmatrix} = -\begin{pmatrix} {}^{k_{\max}}\delta\mathbf{g}^{(2N-1)\times 1} \\ {}^{k_{\max}-1}\delta\mathbf{g}^{(2N-1)\times 1} \\ \vdots \\ {}^2\delta\mathbf{g}^{(2N-1)\times 1} \\ \delta\mathbf{h}^{N\times 1} \end{pmatrix}. \tag{56}$$

We note that the independent solution matrices $\mathcal{R}$ and $\mathcal{L}$ here are the same as those used in the lowest order theory.

The solutions ${}^k\delta\mathbf{c}$ can be obtained from Eq. (56) by the direct matrix inversion, or equivalently by the following recurrence relations:

$$
\begin{aligned}
{}^{k_{\max}-1}\delta\mathbf{c} &= \mathcal{R}^{-1}\ {}^{k_{\max}}\mathcal{L}.{}^{k_{\max}}\delta\mathbf{c} + \mathcal{R}^{-1}\cdot{}^{k_{\max}}\delta\mathbf{g},\\
{}^{k}\delta\mathbf{c} &= (\mathcal{R}^{-1}\mathcal{L})^{k_{\max}-k-1}\ \mathcal{R}^{-1}{}^{k_{\max}}\mathcal{L}\cdot{}^{k_{\max}}\delta\mathbf{c}\\
&\quad + (\mathcal{R}^{-1}\mathcal{L})^{k_{\max}-k-1}\mathcal{R}^{-1}\cdot{}^{k_{\max}-1}\delta\mathbf{g}\\
&\quad + \sum_{i=k}^{k_{\max}-2}(\mathcal{R}^{-1}\mathcal{L})^{i-k}\mathcal{R}^{-1}.{}^{i+1}\delta\mathbf{g},\\
&\quad \text{for } k = 1,\cdots,k_{\max}-2,
\end{aligned}
$$

where

$$
\begin{aligned}
{}^{k_{\max}}\delta\mathbf{c} &= -[(\mathcal{R}^{-1}\mathcal{L})^{k_{\max}-2}\ \mathcal{R}^{-1}{}^{k_{\max}}\mathcal{L}]^{-1}\\
&\quad \times [[\mathcal{F}\mathcal{L}_d + (\mathcal{K}-\mathcal{V})\mathcal{L}_0]^{-1}\delta\mathbf{h}\\
&\quad + (\mathcal{R}^{-1}\mathcal{L})^{k_{\max}-2}\mathcal{R}^{-1}\cdot{}^{k_{\max}}\delta\mathbf{g}\\
&\quad + \sum_{i=1}^{k_{\max}-2}(\mathcal{R}^{-1}\mathcal{L})^{i-1}\mathcal{R}^{-1}\cdot{}^{i+1}\delta\mathbf{g}].
\end{aligned}
$$

As soon as the solutions of Eq. (56), ${}^{k}\delta\mathbf{c}$, are obtained, the first order eigen function is determined by Eq. (52).

Note that the fixed boundary ballooning mode theory can be regarded as a special case of free boundary one. The lowest and first order theory in this paper can also be generalized to the fixed boundary ballooning mode case. One of the distinguished features of the current formalism of fixed boundary ballooning modes lies in that the applicability of the lowest order stability criterion does not depend on the convergency of the first order solution. This is different from the conventional WKB approach, for example, in Ref. 1. The comparison of current perturbation theory with the conventional WKB type of formulation will be further exploited in the future numerical application of current theory.

VI. CONCLUSIONS AND DISCUSSION

In this paper, we found a new type of ballooning invariance: the invariance of the independent solutions for high n mode equations. This is different from the conventional ballooning invariance: the invariance of the Fourier components of high n modes. The conventional ballooning invariance requires both the equations and boundary conditions to be translationally invariant. The free boundary ballooning formalism developed in this paper requires only the invariance of the governing equations. The translational invariance of the fundamental independent solutions can be derived directly from the invariance of equations. The invariance of the independent solutions is more fundamental and can be used to treat external modes. Using this newly discovered invariance, it is shown that the 2D external ballooning mode problem can be reduced to a 1D problem.

To construct the 1D formalisms for both internal and external ballooning modes, one needs only to calculate the independent solutions in a single interval, which is equivalent to a 1D calculation. In the internal ballooning mode case, these independent solutions are used to fit the boundary conditions at both ends of the interval. In the external ballooning mode case these independent solutions are used to fit the boundary conditions at plasma core and plasma-vacuum interface and the continuity conditions between nearby intervals. Comparing with the internal ballooning mode calculation, the extra amount of calculation for external ballooning modes is about the calculation of the recurrence equations in Eqs. (36)–(38). Counting in this extra calculation, one may regard it as a quasi-1D problem.

In difference from the procedure in Refs. 5 and 6, which consider only the next order correction for the envelope due to the free boundary. The current formalism taps the invariance property in the lowest order. From the interchange mode theory, we know that each Fourier components behaves at their respective resonance surfaces $(x-M)\to 0$ as follows:[7]

$$u_m \to (x-M)^{-1/2\pm\sqrt{-D_I}},$$

where D_I is the Mercier index and $\pm$ sign depends on the position of the resonance surfaces for individual Fourier components. If the mode resonance surface $(x-M)=0$ resides inside the plasma region, only the positive-sign solution (i.e., the so-called small solution) is allowed, since the negative-sign solution (i.e., the so-called large solution) can lead the energy integral $\int |u_m|^2\,dx$ to diverge. However, in the case with the resonance surface residing in the vacuum region the large solution is acceptable. As a matter of fact, the minimization of the total energy of plasma, vacuum, and surface contributions leads the large solution to prevail, if the resonance surface resides in the vacuum region. It is because of the presentation of large solution that a more stringent stability criterion for peeling modes is obtained.[8,9] This indicates that each Fourier component can behave quite differently according to the locations of their respective resonance surfaces $(x-M)$, inside or outside plasma region. Furthermore, using the transform $t_m = 1/(x-M)$, one can prove that the infinite legs $(x-M\to -\infty)$ have similar behavior as the resonance surfaces $(x-M=0)$. The Fourier components differs in accordance with how much their infinite legs extend into the vacuum region. Similarly, another type of peeling modes occurs when the infinite leg contains the large solution.[8,9] This shows that even for those Fourier components with their resonance surfaces residing inside plasma region they are not invariant. Therefore, using the conventional ballooning invariance in Refs. 5 and 6 for free boundary modes can cause the peeling effect to be left out in the leading order. In our theory the translational invariance is applied to the independent solutions, which contain both the large and small solutions, therefore, the peeling mode effects are taken into account to the leading order.

For the internal ballooning modes, the amplitudes of each Fourier component remain the same in the leading order, as shown in Fig. 2. The envelope of the amplitudes of leading order is determined by the next order effects, by taking into account the slow variances of equilibrium quantities.[1,2] This is different for peeling ballooning modes. Since the distance between the respective resonance surface of individual Fourier component and the plasma-vacuum interface determines how much the peeling energy of individual

Fourier harmonic can be released, various types of envelopes can develop naturally by the energy minimization of the leading order, without taking into consideration the slow variances of equilibrium quantities. For example, Fig. 5 can be interpreted as follows: the envelope of decaying type toward plasma core of six visible resonance peaks are due to their extensions of $x-M\to-\infty$ legs in the vacuum region becoming shorter and shorter. From the peeling mode theory of this type,[9] we know that the shorter the leg in the vacuum region, the less the peeling energy can be released. This results in the decaying type of envelope in Fig. 5. This feature tells the key difference of the current formalism from that in Ref. 5.

In this paper, we also develop the first order theory to include the effects of slow equilibrium variance. This is different from the conventional WKB formalism in Refs. 1 and 5. One of the distinguished features of the current formalism lies in that the applicability of the lowest order stability criterion does not depend on the convergency of the first order solution.

Since the current formalism is adaptable to the cases with various sharp boundary changes, it therefore can be also generalized to study the piece-wise equilibrium cases. For example, the H-mode pedestal can be modeled approximately by two sets of independent solutions: one for pedestal top and inward region and the other for pedestal region. By suitable matching procedure, the 2D problem can be reduced to two 1D problems. Similarly, the current formalism can also be applied to study the X-point effect. In the presence of X-point the magnetic shear becomes infinite toward to the X-point. This case is difficult to be handled by the existing 2D codes. The current 1D approach may offer an approximate solution for it. Introducing a set of independent solutions for the region at the vicinity of X-point and using them to match the independent solutions in the plasma core, one can also reduce to this type of complicated 2D problem to a few 1D problems. Further applications remain to be exploited in the future.

ACKNOWLEDGMENTS

This research was supported by U. S. Department of Energy, Office of Fusion Energy Science.

APPENDIX: EXPLANATION OF THE FREE BOUNDARY BALLOONING FORMALISM IN A REDUCED MODEL

Let us use the case with single sideband coupling from either side and with only three resonance surfaces involved to explain the free boundary ballooning formalism in the main text.

As shown in Fig. 1, the three regions are labeled as follows: the 1st region: $\Delta\to1+\Delta$, containing the resonance surface m_0/n; the 2nd region: $1+\Delta\to2+\Delta$, containing the resonance surface $(m_0-1)/n$; and the 3rd one: $2+\Delta\to3+\Delta$, containing the resonance surface $(m_0-2)/n$. In this model only three Fourier harmonics are present in each region: in the 1st region they are $(m_0+1)/n$, m_0/n, and $(m_0-1)/n$; in the 2nd region they are m_0/n, $(m_0-1)/n$, and $(m_0-2)/n$; and in the 3rd region they are $(m_0-1)/n$, $(m_0-2)/n$, and $(m_0-3)/n$ components.

One can compute the independent solutions for three components: $(m_0+1)/n$, m_0/n, $(m_0-1)/n$ in the 1st region $\Delta\to1+\Delta$. Since they are three coupled 2nd order differential equation (3), they can be transformed to a set of six first order differential equations. Their solutions can be expressed as a vector:

$$\begin{pmatrix} u_{m_0+1} \\ \frac{du_{m_0+1}}{dx} \\ u_{m_0} \\ \frac{du_{m_0}}{dx} \\ u_{m_0-1} \\ \frac{du_{m_0-1}}{dx} \end{pmatrix}. \tag{A1}$$

When the following six initial conditions

$$\begin{pmatrix}1\\0\\0\\0\\0\\0\end{pmatrix},\ \begin{pmatrix}0\\1\\0\\0\\0\\0\end{pmatrix},\ \begin{pmatrix}0\\0\\1\\0\\0\\0\end{pmatrix},\ \begin{pmatrix}0\\0\\0\\1\\0\\0\end{pmatrix},\ \begin{pmatrix}0\\0\\0\\0\\1\\0\end{pmatrix},\ \begin{pmatrix}0\\0\\0\\0\\0\\1\end{pmatrix} \tag{A2}$$

are given at the right end of the 1st region $x=1-\Delta$, one can get the six independent solutions by shooting respectively from $x=1-\Delta$ to $x=\Delta$

$$\begin{pmatrix} u_{m_0+1} \\ \frac{du_{m_0+1}}{dx} \\ u_{m_0} \\ \frac{du_{m_0}}{dx} \\ u_{m_0-1} \\ \frac{du_{m_0-1}}{dx} \end{pmatrix}_1,\ \begin{pmatrix} u_{m_0+1} \\ \frac{du_{m_0+1}}{dx} \\ u_{m_0} \\ \frac{du_{m_0}}{dx} \\ u_{m_0-1} \\ \frac{du_{m_0-1}}{dx} \end{pmatrix}_2,\ \begin{pmatrix} u_{m_0+1} \\ \frac{du_{m_0+1}}{dx} \\ u_{m_0} \\ \frac{du_{m_0}}{dx} \\ u_{m_0-1} \\ \frac{du_{m_0-1}}{dx} \end{pmatrix}_3,$$

$$\begin{pmatrix} u_{m_0+1} \\ \frac{du_{m_0+1}}{dx} \\ u_{m_0} \\ \frac{du_{m_0}}{dx} \\ u_{m_0-1} \\ \frac{du_{m_0-1}}{dx} \end{pmatrix}_4,\ \begin{pmatrix} u_{m_0+1} \\ \frac{du_{m_0+1}}{dx} \\ u_{m_0} \\ \frac{du_{m_0}}{dx} \\ u_{m_0-1} \\ \frac{du_{m_0-1}}{dx} \end{pmatrix}_5,\ \begin{pmatrix} u_{m_0+1} \\ \frac{du_{m_0+1}}{dx} \\ u_{m_0} \\ \frac{du_{m_0}}{dx} \\ u_{m_0-1} \\ \frac{du_{m_0-1}}{dx} \end{pmatrix}_6. \tag{A3}$$

The general solution in the 1st region can be written as the linear combination of the independent solutions

$$\begin{pmatrix} u_{m_0+1} \\ \frac{du_{m_0+1}}{dx} \\ u_{m_0} \\ \frac{du_{m_0}}{dx} \\ u_{m_0-1} \\ \frac{du_{m_0-1}}{dx} \end{pmatrix} = {}^1c_1 \begin{pmatrix} u_{m_0+1} \\ \frac{du_{m_0+1}}{dx} \\ u_{m_0} \\ \frac{du_{m_0}}{dx} \\ u_{m_0-1} \\ \frac{du_{m_0-1}}{dx} \end{pmatrix}_1 + {}^1c_2 \begin{pmatrix} u_{m_0+1} \\ \frac{du_{m_0+1}}{dx} \\ u_{m_0} \\ \frac{du_{m_0}}{dx} \\ u_{m_0-1} \\ \frac{du_{m_0-1}}{dx} \end{pmatrix}_2 + {}^1c_3 \begin{pmatrix} u_{m_0+1} \\ \frac{du_{m_0+1}}{dx} \\ u_{m_0} \\ \frac{du_{m_0}}{dx} \\ u_{m_0-1} \\ \frac{du_{m_0-1}}{dx} \end{pmatrix}_3 + {}^1c_4 \begin{pmatrix} u_{m_0+1} \\ \frac{du_{m_0+1}}{dx} \\ u_{m_0} \\ \frac{du_{m_0}}{dx} \\ u_{m_0-1} \\ \frac{du_{m_0-1}}{dx} \end{pmatrix}_4 + {}^1c_5 \begin{pmatrix} u_{m_0+1} \\ \frac{du_{m_0+1}}{dx} \\ u_{m_0} \\ \frac{du_{m_0}}{dx} \\ u_{m_0-1} \\ \frac{du_{m_0-1}}{dx} \end{pmatrix}_5 + {}^1c_6 \begin{pmatrix} u_{m_0+1} \\ \frac{du_{m_0+1}}{dx} \\ u_{m_0} \\ \frac{du_{m_0}}{dx} \\ u_{m_0-1} \\ \frac{du_{m_0-1}}{dx} \end{pmatrix}_6, \tag{A4}$$

where ${}^1c_i$ $(i=1,\ldots,6)$ are constants to be determined by the boundary and matching conditions.

With the same boundary conditions in Eq. (A2) applied respectively for the right ends of the 2nd and 3rd regions, one can expect the independent solutions in the 2nd and 3rd regions are translationally invariant to those in the 1st region in Eq. (A3) with shifted mode numbers. Consequently, the general solutions in the 2nd and 3rd regions can be expressed respectively as follows:

$$\begin{pmatrix} u_{m_0} \\ \frac{du_{m_0}}{dx} \\ u_{m_0-1} \\ \frac{du_{m_0-1}}{dx} \\ u_{m_0-2} \\ \frac{du_{m_0-2}}{dx} \end{pmatrix} = {}^2c_1 \begin{pmatrix} u_{m_0} \\ \frac{du_{m_0}}{dx} \\ u_{m_0-1} \\ \frac{du_{m_0-1}}{dx} \\ u_{m_0-2} \\ \frac{du_{m_0-2}}{dx} \end{pmatrix}_1 + {}^2c_2 \begin{pmatrix} u_{m_0} \\ \frac{du_{m_0}}{dx} \\ u_{m_0-1} \\ \frac{du_{m_0-1}}{dx} \\ u_{m_0-2} \\ \frac{du_{m_0-2}}{dx} \end{pmatrix}_2 + {}^2c_3 \begin{pmatrix} u_{m_0} \\ \frac{du_{m_0}}{dx} \\ u_{m_0-1} \\ \frac{du_{m_0-1}}{dx} \\ u_{m_0-2} \\ \frac{du_{m_0-2}}{dx} \end{pmatrix}_3 + {}^2c_4 \begin{pmatrix} u_{m_0} \\ \frac{du_{m_0}}{dx} \\ u_{m_0-1} \\ \frac{du_{m_0-1}}{dx} \\ u_{m_0-2} \\ \frac{du_{m_0-2}}{dx} \end{pmatrix}_4 + {}^2c_5 \begin{pmatrix} u_{m_0} \\ \frac{du_{m_0}}{dx} \\ u_{m_0-1} \\ \frac{du_{m_0-1}}{dx} \\ u_{m_0-2} \\ \frac{du_{m_0-2}}{dx} \end{pmatrix}_5 + {}^2c_6 \begin{pmatrix} u_{m_0} \\ \frac{du_{m_0}}{dx} \\ u_{m_0-1} \\ \frac{du_{m_0-1}}{dx} \\ u_{m_0-2} \\ \frac{du_{m_0-2}}{dx} \end{pmatrix}_6, \tag{A5}$$

$$\begin{pmatrix} u_{m_0-1} \\ \frac{du_{m_0-1}}{dx} \\ u_{m_0-2} \\ \frac{du_{m_0-2}}{dx} \\ u_{m_0-3} \\ \frac{du_{m_0-3}}{dx} \end{pmatrix} = {}^3c_1 \begin{pmatrix} u_{m_0-1} \\ \frac{du_{m_0-1}}{dx} \\ u_{m_0-2} \\ \frac{du_{m_0-2}}{dx} \\ u_{m_0-3} \\ \frac{du_{m_0-3}}{dx} \end{pmatrix}_1 + {}^3c_2 \begin{pmatrix} u_{m_0-1} \\ \frac{du_{m_0-1}}{dx} \\ u_{m_0-2} \\ \frac{du_{m_0-2}}{dx} \\ u_{m_0-3} \\ \frac{du_{m_0-3}}{dx} \end{pmatrix}_2 + {}^3c_3 \begin{pmatrix} u_{m_0-1} \\ \frac{du_{m_0-1}}{dx} \\ u_{m_0-2} \\ \frac{du_{m_0-2}}{dx} \\ u_{m_0-3} \\ \frac{du_{m_0-3}}{dx} \end{pmatrix}_3 + {}^3c_4 \begin{pmatrix} u_{m_0-1} \\ \frac{du_{m_0-1}}{dx} \\ u_{m_0-2} \\ \frac{du_{m_0-2}}{dx} \\ u_{m_0-3} \\ \frac{du_{m_0-3}}{dx} \end{pmatrix}_4 + {}^3c_5 \begin{pmatrix} u_{m_0-1} \\ \frac{du_{m_0-1}}{dx} \\ u_{m_0-2} \\ \frac{du_{m_0-2}}{dx} \\ u_{m_0-3} \\ \frac{du_{m_0-3}}{dx} \end{pmatrix}_5 + {}^3c_6 \begin{pmatrix} u_{m_0-1} \\ \frac{du_{m_0-1}}{dx} \\ u_{m_0-2} \\ \frac{du_{m_0-2}}{dx} \\ u_{m_0-3} \\ \frac{du_{m_0-3}}{dx} \end{pmatrix}_6, \tag{A6}$$

where ${}^{1,2}c_i$ $(i=1,\ldots,6)$ are constants.

Note that the general solutions in Eqs. (A4)–(A6) for three regions contain 18 constants: ${}^1c_1, {}^1c_2, {}^1c_3, {}^1c_4, {}^1c_5, {}^1c_6, {}^2c_1, {}^2c_2, {}^2c_3, {}^2c_4, {}^2c_5, {}^2c_6, {}^3c_1, {}^3c_2, {}^3c_3, {}^3c_4, {}^3c_5, {}^3c_6$. One also has the same number of boundary and matching conditions: (a) the 3 boundary conditions at plasma-vacuum interface $x=\Delta$; (b) the 3 boundary conditions at the plasma core $x=3-\Delta$; (c) the 6 matching conditions at the region

interface $x = 1 - \Delta$; (d) the 6 matching conditions at the region interface $x = 2 - \Delta$. Therefore, the 18 constants can be determined completely by the boundary and matching conditions. This constitutes the eigenvalue problem for determining the so-called peeling-ballooning modes. These constants determine not only the behavior of individual Fourier components, but also the envelope in the leading order. This is different from the conventional ballooning mode theory, in which the only envelope shape determined in the leading order is the so-called θ_k effect.

As explained in Sec. III through Figs. 3 and 4, the general solution in the 1st region in Eq. (A4) is obtained through a computation that is equivalent to a 1D calculation. The general solutions in the 2nd and 3rd regions in Eqs. (A5) and (A6) are obtained through applying the invariance property in Eq. (24) and no additional computation is required. This shows how the 2D free boundary ballooning mode problem is reduced to a 1D problem. Here, we have outlined the underlying thoughts in a reduced model. The general formalism is described in the main text.

[1]J. W. Connor, R. J. Hastie, and J. B. Taylor, Proc. R. Soc. London, Ser. A **365**, 1 (1979).
[2]Y. C. Lee and J. W. Van Dam, in *Proceedings of the Finite Beta Theory Workshop*, edited by B. Coppi and W. Sadowski (U. S. Department of Energy, Washington, D.C., 1977), p. 93.
[3]A. H. Glasser, in *Proceedings of the Finite Beta Theory Workshop*, edited by B. Coppi and W. Sadowski (U. S. Department of Energy, Washington, D.C., 1977), p. 55.
[4]R. D. Hazeltine, D. A. Hitchcock, and S. M. Mahajan, Phys. Fluids **24**, 180 (1981).
[5]J. W. Connor, R. J. Hastie, H. R. Wilson, and R. L. Miller, Phys. Plasmas **5**, 2687 (1998).
[6]J. J. Ramos, R. Verastegui, and R. J. Hastie, Phys. Plasmas **8**, 2029 (2001).
[7]J. M. Greene and J. L. Johnson, Phys. Fluids **5**, 510 (1962).
[8]D. Lortz, Nucl. Fusion **15**, 49 (1975).
[9]J. A. Wesson, Nucl. Fusion **18**, 87 (1978).
[10]R. Fitzpatrick, R. J. Hastie, T. J. Martin, and C. M. Roach, Nucl. Fusion **33**, 1533 (1993).
[11]D. Lortz and J. Nührenberg, Phys. Lett. A **68**, 49 (1978).
[12]L.-J. Zheng and M. Kotschenreuther, J. Comput. Phys. **211**, 748 (2006).
[13]A. H. Glasser, "The direct criterion of Newcomb for the stability of an axisymmetric toroidal plasma," Los Alamos Report: LA-UR-95-528, 1997.